Effective Lifetime of Non-Equilibrium Carriers in Semiconductors from Non-Adiabatic Molecular Dynamics Simulations

Shanshan Wang
Fudan University
Menglin Huang
Fudan University
Yu-Ning Wu
East China Normal University
Weibin Chu
Fudan University
Jin Zhao
University of Science & Technology of China https://orcid.org/0000-0003-1346-5280
Aron Walsh
Imperial College London https://orcid.org/0000-0001-5460-7033
Xin-Gao Gong
Fudan University
Su-Huai Wei
Beijing Computational Science Research Center
Shiyou Chen (chensy@fudan.edu.cn)
Fudan University https://orcid.org/0000-0002-4039-8549

Article

Keywords:

Posted Date: March 2nd, 2022

DOI: https://doi.org/10.21203/rs.3.rs-1366420/v1

Version of Record: A version of this preprint was published at Nature Computational Science on August 22nd, 2022. See the published version at https://doi.org/10.1038/s43588-022-00297-y.

Effective Lifetime of Non-Equilibrium Carriers in Semiconductors from Non-Adiabatic Molecular Dynamics Simulations

Shanshan Wang[1,2], Menglin Huang[1], Yu-Ning Wu[2], Weibin Chu[1], Jin Zhao[3], Aron Walsh[4], Xin-Gao Gong[1,5], Su-Huai Wei[6], and Shiyou Chen[1,2,5,*]

[1]Key Laboratory of Computational Physical Sciences (MOE), and State Key Laboratory of ASIC and System, School of Microelectronics, Fudan University, Shanghai 200433, China, *chensy@fudan.edu.cn
[2]Key Laboratory of Polar Materials and Devices (MOE) and Department of Electronics, East China Normal University, Shanghai 200241, China
[3]ICQD/Hefei National Laboratory for Physical Sciences at the Microscale, CAS Key Laboratory of Strongly-Coupled Quantum Matter Physics, and Department of Physics, University of Science and Technology of China, Hefei, Anhui 230026, China
[4]Department of Materials, Imperial College London, Exhibition Road, London SW7 2AZ, UK
[5]Shanghai Qi Zhi Institute, Shanghai 200030, China
[6]Beijing Computational Science Research Center, Beijing 100193, China

The lifetime of non-equilibrium electrons and holes in semiconductors is crucial for solar cell and optoelectronic applications. Non-adiabatic molecular dynamics (NAMD) simulations based on time-dependent density functional theory (TDDFT) are widely used to study excited-state carrier dynamics. However, the calculated carrier lifetimes are often different from experimental results by orders of magnitude. In this work, by revisiting the definition of carrier lifetime and considering different recombination mechanisms, we report a systematic procedure for calculating the effective carrier lifetime in realistic semiconductor crystals that can be compared directly to experimental measurements. The procedure shows that considering all recombination mechanisms and using reasonable densities of carriers and defects are crucial in calculating the effective lifetime. When NAMD simulations consider only Shockey-Read-Hall (SRH) defect-assisted and band-to-band non-radiative recombination while neglect band-to-band radiative recombination, and the densities of non-equilibrium carriers and defects in supercell simulations are much higher than those in realistic semiconductors under solar illumination, the calculated lifetimes are ineffective and thus differ from experiments. Using our procedure, the calculated effective lifetime of the halide perovskite $CH_3NH_3PbI_3$ agrees with experiments. It is mainly determined by band-to-band radiative and defect-assisted non-radiative recombination, while band-to-band non-radiative recombination is negligible. These results indicate that it is possible to calculate carrier lifetimes accurately based on NAMD simulations, but the directly calculated values should be converted to effective lifetimes for comparison to experiments. The revised procedure can be widely applied in future carrier lifetime simulations.

Excited-state carrier dynamics in semiconductors is fundamental to the development of optoelectronic[1], photovoltaic[2], photocatalytic[3] and other functional devices working under light illumination. The lifetime of the photo-excited non-equilibrium carriers is an important quantity determining the performance of these devices, *e.g.*, it determines the diffusion length of the minority carriers in photovoltaic semiconductors and is thus critical to the efficiency of solar cells. For decades, this important quantity is obtained mainly through the ultrafast time-resolved photoluminescence spectroscopy[4] and transient absorption spectroscopy[5,6].

Theoretically, conventional first-principles molecular dynamics based on adiabatic approximation does not describe the excited-state carrier dynamics. However, rapid developments in nonadiabatic molecular dynamics (NAMD)[7,8] based on time-dependent DFT (TDDFT)[9] methods in the past decade has made the simulation of excited-state carrier dynamics in semiconductors possible. A series of breakthroughs have been reported recently[10-20]. Therefore, the first-principles prediction of carrier lifetime is attracting wide attention. There are many groups worldwide who have adopted the NAMD simulations based on Erhenfest or surface hopping schemes to predict the lifetime of non-equilibrium carriers[21-42]. In these studies, non-equilibrium carrier populations were produced by exciting an electron from the occupied level to a higher-energy unoccupied level in the supercell calculations, *e.g.*, from the valence band maximum (VBM) level to the conduction band minimum (CBM) level. Then NAMD simulations were performed and the lifetime τ was calculated through fitting the decay of the electron population on the excited-state level to the function $\Delta n(t) \propto \exp(-t/\tau)$ [21-42]. For example, the NAMD simulation of Qiao *et al.* predicted that the lifetime of photo-excited carriers is 1.5 ns in $CH_3NH_3PbI_3$[43], and similar values were reported in other studies[44-47]. However, plenty of experiments have reported that the actual lifetime of photo-excited carriers can be as long as several microseconds in $CH_3NH_3PbI_3$[48-52]. There is a discrepancy between the calculated and experimental values.

To reveal the origin of the discrepancy, we repeated the NAMD simulation using the procedures as in Ref. [43] and found that our result agrees with theirs, so technical errors in the simulations can be excluded. Kim and Walsh pointed out that non-adiabatic coupling matrix elements between the valence and conduction bands may be significantly overestimated in the NAMD simulations, which results in exaggerated

non-radiative recombination in pristine $CH_3NH_3PbI_3$ and thus causes the short lifetime[53]. That means the accuracy issues of the current NAMD methods may be one possible origin of the discrepancy. On the other hand, as noted by Qiao *et al.*[43] and Chu *et al.*[54], most of the present NAMD simulations used supercells with a limited size, so the simulations assumed a certain carrier density, defect density, and light intensity, which might be very different from the conditions in real samples and can thus also be the origin of the discrepancy. If this is the origin, then two open questions appear: (i) what is the meaning of the directly calculated carrier lifetime from the NAMD simulations; (ii) is it possible to use the NAMD simulations to calculate the carrier lifetime that can be compared directly to the experimentally measured lifetime of the real semiconductor samples with the actual carrier density and defect density, and working under solar illumination?

In this work, we started from the fundamental definition of the lifetime of non-equilibrium carriers and developed a systematic procedure for calculating the effective carrier lifetime in real samples based on the results from the NAMD simulations and other calculations. The calculated effective carrier lifetime can be compared directly to experimental values. Using this procedure, we find that the reported lifetime (1.5 ns) of $CH_3NH_3PbI_3$ in previous NAMD studies is the seriously underestimated lifetime $\tau_{band-band}^{non-rad}$ of band-to-band non-radiative recombination, and the effective $\tau_{band-band}^{non-rad}$ is actually very long (150 μs). The effective carrier lifetime in $CH_3NH_3PbI_3$ is mainly determined by the band-to-band radiative and defect-assisted SRH recombination, while the influence of band-to-band non-radiative recombination is negligible. When all recombination mechanisms are considered and the effects are summed using the systematic procedure, the effective lifetime is consistent with the experimental lifetime and can explain the observed efficient photoluminescence of $CH_3NH_3PbI_3$. Besides that, we also revisited the carrier lifetime of three other optoelectronic semiconductors reported in recent NAMD studies and found that the conclusions can be changed if all the recombination mechanisms are considered and reasonable carrier and defect densities are used in the simulation. We propose that it is necessary to calculate the effective lifetime using the systematic procedure outlined here in future carrier dynamics studies to provide the correct understanding of the mechanisms that determine the experimentally measured carrier lifetime.

Methods

Definition of Carrier Lifetime and Systematic Calculation Procedure.

As discussed in many textbooks of semiconductor physics[55], the time derivative of the non-equilibrium carrier density $\Delta n(t)$ is equal to the difference between the generation rate *G* and the recombination rate *U* of non-equilibrium carriers,

$$\frac{d\Delta n(t)}{dt} = G(t) - U(t) \qquad (1).$$

When the generation stops, *G(t)*=0, $\Delta n(t)$ will decay with the rate -*U(t)*. If the recombination rate $U(t)$ depends linearly on $\Delta n(t)$, *i.e.*,

$$U(t) = \frac{\Delta n(t)}{\tau} \qquad (2)$$

where τ is a constant,

$$\tau = \frac{\Delta n(t)}{U(t)} \qquad (3),$$

then the decay of $\Delta n(t)$ will follow,

$$\Delta n(t) = \Delta n(0)\exp\left(-\frac{U(t)}{\Delta n(t)}t\right) = \Delta n(0)\exp(-\frac{t}{\tau}) \qquad (4)$$

where $\Delta n(0)$ is the density of non-equilibrium carriers at the *t* = 0 moment when the generation stops. As we can see, in this case, the constant τ means the time when the density decays to *1/e* of the original value $\Delta n(0)$ after the generation stops, so it is defined as the lifetime of non-equilibrium carriers. Then, Eq. (1) becomes,

$$\frac{d\Delta n(t)}{dt} = -U(t) = -\frac{\Delta n(t)}{\tau} \qquad (5).$$

In standard NAMD studies, the lifetime τ is calculated through fitting the decay of the electron population on the excited-state level to the function $P(t) \propto \exp(-t/\tau)$, which originates from the decay function Eq. (4).

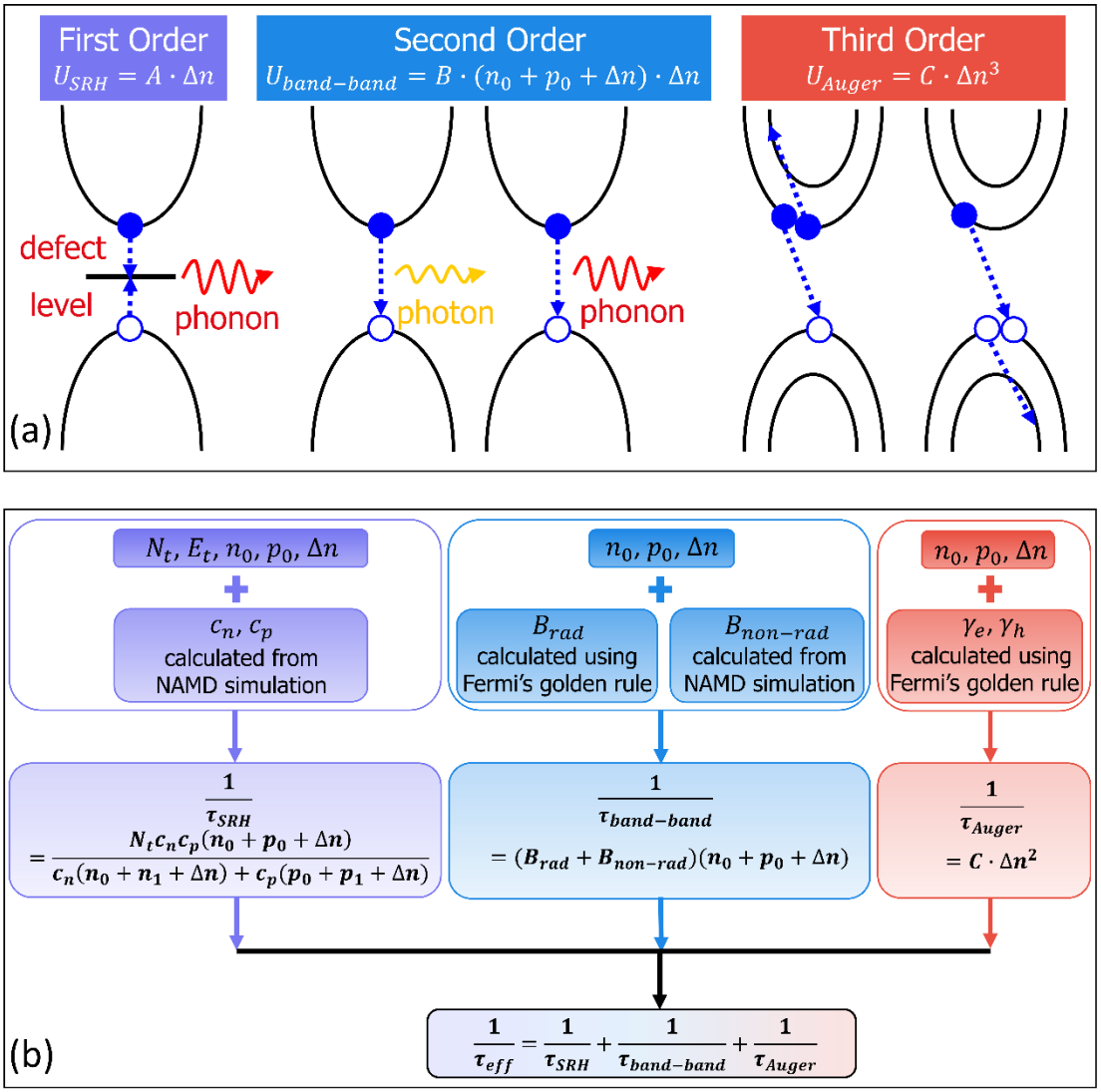

Figure 1. The schematic plot of the first-order defect-assisted SRH, the second-order band-to-band radiative or non-radiative, and the third-order Auger recombination (a), and the procedure for calculating the effective lifetime with the three major recombination mechanisms considered (b).

According to Eq. (3), the lifetime τ is determined by the ratio between the density of non-equilibrium carriers $\Delta n(t)$ and the recombination rate *U(t)*. In semiconductors, as shown in Fig. 1(a), there are many possible recombination mechanisms, *e.g.*, the defect-assisted non-radiative SRH recombination, the band-to-band recombination, and the Auger recombination. Therefore, the recombination rate *U(t)* is the sum of the rates of all these mechanisms,

$$U(t) = U_{SRH}(t) + U_{band-band}(t) + U_{Auger}(t) \qquad (6).$$

Correspondingly, the lifetime that is effective in real semiconductor samples should also be contributed by all these mechanisms,

$$\frac{1}{\tau} = \frac{1}{\tau_{SRH}} + \frac{1}{\tau_{band-band}} + \frac{1}{\tau_{Auger}} \qquad (7)$$

where τ_{SRH}, $\tau_{band-band}$ and τ_{Auger} are the lifetime when only one of the three mechanisms are considered. With this definition, we can also write,

$$\tau_{SRH} = \frac{\Delta n(t)}{U_{SRH}} \qquad (8),$$

$$\tau_{band-band} = \frac{\Delta n(t)}{U_{band-band}} \qquad (9),$$

$$\tau_{Auger} = \frac{\Delta n(t)}{U_{Auger}} \qquad (10).$$

As shown in Refs. [55] for photo-excited non-equilibrium carriers (the densities of non-equilibrium electrons and holes are equal, $\Delta n(t) = \Delta p(t)$), the three recombination rates depend not only on $\Delta n(t)$, but also on the electron carrier density n_0 and hole carrier density p_0 under the equilibrium state, as described by,

$$U_{SRH}(t) = A \cdot \Delta n(t) \qquad (11),$$

$$U_{band-band}(t) = \Delta n(t) \cdot B \cdot [n_0 + p_0 + \Delta n(t)] \qquad (12),$$

$$U_{Auger}(t) = C \cdot \Delta n(t)^3 \qquad (13)$$

in which, *A*, *B* and *C* are the SRH defect-assisted non-radiative, band-to-band and Auger recombination coefficients, respectively; n_0 and p_0 can be calculated as $n_0 = N_c exp\,(\frac{E_F - E_{CBM}}{k_0 T})$ and $p_0 = N_v \exp\,(\frac{E_{VBM} - E_F}{k_0 T})$, where T is the temperature, k_0 is the Boltzmann constant, E_F is the Fermi level, E_{VBM} is the valence band maximum level, E_{CBM} is the conduction band minimum level, and N_v and N_c are the effective density of states for valence band and conduction band edges, respectively.

The SRH recombination coefficient *A* can be calculated following[56-58],

$$A = \frac{N_t c_n c_p (n_0 + p_0 + \Delta n(t))}{c_n (n_0 + n_1 + \Delta n(t)) + c_p (p_0 + p_1 + \Delta n(t))} \qquad (14)$$

where N_t is the density of the recombination-center defects; c_n and c_p are the electron capture coefficient and hole capture coefficient of the defect level, respectively; $n_1 =$

$N_c exp\ (\frac{E_t - E_{CBM}}{k_0 T})$, $p_1 = N_v \exp\ (\frac{E_{VBM} - E_t}{k_0 T})$ in which E_t is the energy of defect level.

The Auger recombination coefficient *C* can be calculated following[55],

$$C = \frac{(\gamma_e n_0 + \gamma_h p_0)[n_0 + p_0 + \Delta n(t)] + (\gamma_e + \gamma_h)[n_0 + p_0 + \Delta n(t)]\Delta n(t)}{\Delta n(t)^2} \quad (15)$$

in which γ_e and γ_h represent the *e-e-h* Auger recombination coefficient (one electron at the conduction band is excited to higher-level state when one electron-hole pair recombines) and *h-h-e* Auger recombination coefficient (one hole at the valence band is promoted to lower-level state when one electron-hole pair recombines).

According to Eqs. (11-15), we can notice that the recombination rate *U(t)* (including $U_{SRH}(t)$, $U_{band-band}(t)$ and $U_{Auger}(t)$) depends non-linearly on $\Delta n(t)$, so τ (the carrier lifetime) is not a constant with respect to $\Delta n(t)$. Therefore, in principle, the decay of $\Delta n(t)$ does not follow the simple function in Eq. (4). When τ was defined as the carrier lifetime (the time when the density decays to *1/e* of the original value $\Delta n(0)$ after the generation stops) and was calculated through fitting the decay of $\Delta n(t)$ to the function $\exp(-t/\tau)$, we assumed implicitly that τ is a constant and *U(t)* depends linearly on $\Delta n(t)$ in the following recombination processes after the generation stops. Of course, the fitting cannot be good if τ has a strong dependence on $\Delta n(t)$. Therefore, when we discuss the carrier lifetime τ, we must pay attention to this dependence and note that τ can be approximated as a constant only for a small range of *t* in which $\Delta n(t)$ does not change significantly. In such a small range of *t*, $\Delta n(t)$ can be approximated as $\Delta n(0)$ which is the value at the moment when the generation stops. With $\Delta n(0)$, the recombination coefficients *A* and *B* can thus be determined, then the corresponding lifetime can be calculated as,

$$\tau_{SRH} = \frac{1}{A} \quad (16)$$

$$\tau_{band-band} = \frac{1}{B \cdot [n_0 + p_0 + \Delta n(0)]} \quad (17)$$

$$\tau_{Auger} = \frac{1}{(\gamma_e n_0 + \gamma_h p_0)[n_0 + p_0 + \Delta n(0)] + (\gamma_e + \gamma_h)[n_0 + p_0 + \Delta n(0)]\Delta n(0)} \quad (18).$$

In operating devices under continuous illumination, the density of non-equilibrium carriers should reach a steady state after the generation and recombination are counterbalanced, then the steady-state density should be considered as $\Delta n(0)$ when

calculating the carrier lifetime according to Eqs. (16), (17) and (18).

As shown in Fig. 1a, the defect-assisted SRH non-radiative recombination occurs between one carrier (electron or hole) and one defect, so the dependence of U_{SRH} on Δn (abbreviation of $\Delta n(0)$) is first order in Eq. (11); the band-to-band recombination occurs between two carriers (one electron and one hole), so the dependence of $U_{band-band}$ on Δn is second order in Eq. (12); the Auger recombination occurs between three carriers (two electrons and one hole, or one electron and two holes), so the dependence of U_{Auger} on Δn is third order in Eq. (13). Therefore, when the density Δn of photo-excited non-equilibrium carriers is small, U_{SRH} and $U_{band-band}$ are much larger than U_{Auger}, thus τ_{SRH} and $\tau_{band-band}$ determine τ; when Δn is large, U_{SRH} and $U_{band-band}$ are much smaller than U_{Auger}, thus τ_{Auger} determines τ[59].

In order to calculate the total effective lifetime τ of non-equilibrium carriers in real semiconductor samples with a certain defect density N_t, equilibrium carrier density n_0 (p_0), and non-equilibrium carrier density $\Delta n(0)$, τ_{SRH}, $\tau_{band-band}$ and τ_{Auger} should all be calculated and combined. A procedure is plotted in Fig. 1b to show the flow of the calculations, including:

(1) For a given type of defect with the energy level E_t, calculate its electron and hole capture coefficients c_n, c_p. They can be calculated from the NAMD simulation, as discussed in the following section "Dependence of τ_{SRH} on Density of Recombination-Center Defects", or using the non-radiative multi-phonon theory[60,61]. With E_t, c_n and c_p, τ_{SRH} can be calculated for given N_t, n_0 (p_0) and $\Delta n(0)$.

(2) Calculate the band-to-band recombination coefficient B. The detailed methods will be discussed in the following sections "Non-Radiative Carrier Recombination in NAMD Simulations" and "Dependence of $\tau_{band-band}$ on Density of Non-Equilibrium Carriers". With B, $\tau_{band-band}$ can be calculated for given n_0 (p_0) and $\Delta n(0)$.

(3) Calculate the Auger recombination coefficients γ_e and γ_h. The methods have been discussed in Ref. [62]. With γ_e and γ_h, τ_{Auger} can be calculated for given n_0 (p_0) and $\Delta n(0)$.

After the calculation of τ_{SRH}, $\tau_{band-band}$ and τ_{Auger}, the effective lifetime τ can be derived according to Eq. (7) and the value can be compared directly to the

experimentally measured lifetime in real samples with the given N_t, n_0 (p_0) and $\Delta n(0)$.

Results and Discussion

Non-Radiative Recombination in NAMD Simulations.

With the formulae derived for calculating the effective carrier lifetime, now we can analyze why the directly calculated lifetime from the recent NAMD simulations differ from experimental values for $CH_3NH_3PbI_3$.

These simulations adopted supercells with several hundreds of atoms, and considered the cases for both the defect-free supercells and those with defects. For the defect-free supercell, there are no electronic states in the band gap and the recombination occurs between the electron on CBM and the hole on VBM, so the band-to-band recombination is simulated and the derived lifetime is $\tau_{band-band}$. For the supercell with a defect, if a defect level is produced in the band gap, the defect-assisted SRH non-radiative recombination is simulated and the derived lifetime is τ_{SRH}. For both cases, the simulated lifetime ($\tau_{band-band}$ or τ_{SRH}) is only a part of the effective lifetime τ as described by Eq. (7). Incomplete consideration of the recombination mechanisms may cause a large difference between the simulated and experimental results. More importantly, we should pay attention to the dependence of the results on $\Delta n(0)$ and N_t assumed in the simulations. In most simulations, the non-equilibrium electron and hole carriers are generated through exciting an electron from the VBM to CBM in the supercell. If the supercell has several hundred atoms, the density $\Delta n(0)$ of the non-equilibrium carriers is as high as 10^{20} cm^{-3} (for $CH_3NH_3PbI_3$ supercell with 192 atoms, the density is 2.6×10^{20} cm^{-3}). However, under the normal sunlight illumination, the excited non-equilibrium electron carriers have a much lower density, only around 10^{13}-10^{15} cm^{-3} (as calculated below). Obviously, the assumed $\Delta n(0)$ (similarly for the defect density N_t) in the NAMD supercell simulations is much higher than that of the density in real devices working under sunlight illumination, as compared in Fig. 2. Eqs. (16) and (17) show that $\tau_{band-band}$ and τ_{SRH} depend on $\Delta n(0)$ and N_t, so the simulated lifetime actually is the result at the very high $\Delta n(0)$ and N_t, rather than the lifetime in real samples with lower $\Delta n(0)$ and N_t, which is another origin of the large difference.

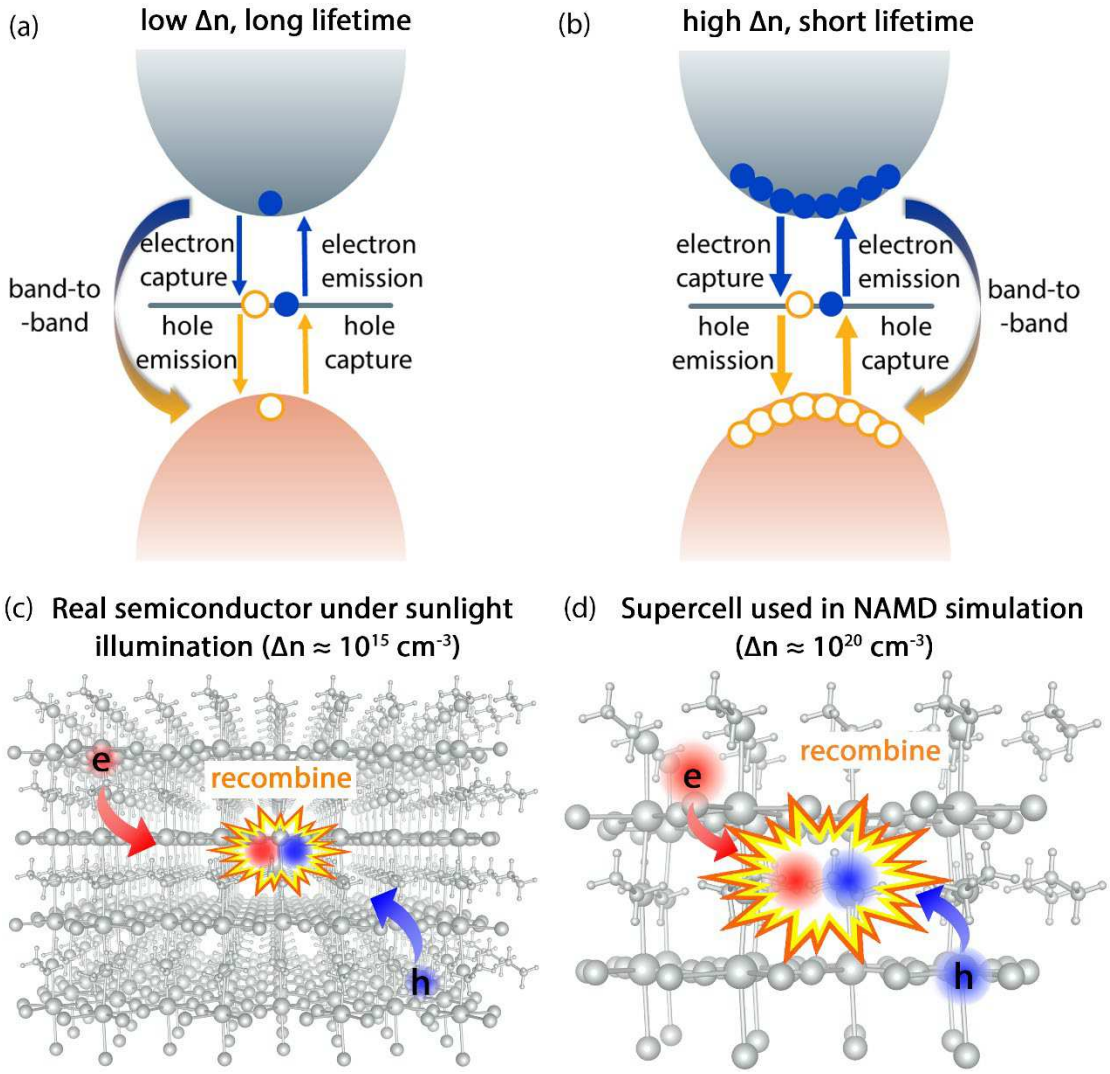

Figure 2. Schematic plot of band-to-band and defect-assisted (SRH) recombination processes in semiconductors with low and high densities of non-equilibrium carriers: (a) and (b) in the reciprocal band-structure space with electron carriers on the conduction band and hole carriers on the valence band; (c) and (d) in the real semiconductor lattice space. The normal density of non-equilibrium carriers is usually around 10^{15} cm^{-3} under sunlight illumination, as shown in (a) and (c), while the density of the non-equilibrium carriers produced in the several-hundred-atom supercell for NAMD simulations can exceed 10^{20} cm^{-3}, as shown in (b) and (d), which causes fast electron-hole recombination.

Attention should also be paid to the meaning of the simulated $\tau_{band-band}$. As shown in Fig. 1a, there are two types of band-to-band recombination: radiative and non-radiative. For band-to-band radiative recombination, the energy of non-equilibrium carriers is converted into the energy of an emitted photon. For band-to-band non-radiative recombination, the energy of non-equilibrium carriers is converted into the

energy of the vibration energy of ions through electron-phonon interactions. The recombination rate and lifetime are contributed by both types, as described by,

$$U_{band-band}(t) = U^{rad}_{band-band}(t) + U^{non-rad}_{band-band}(t)$$

$$= \Delta n(t) \cdot (B_{rad} + B_{non-rad}) \cdot [n_0 + p_0 + \Delta n(t)] \quad (19)$$

$$\frac{1}{\tau_{band-band}} = \frac{1}{\tau^{rad}_{band-band}} + \frac{1}{\tau^{non-rad}_{band-band}} \quad (20).$$

Correspondingly, the recombination coefficient B is also contributed by two parts, B_{rad} and $B_{non-rad}$.

In the standard textbook description, band-to-band recombination is considered as a radiative process,[63] while the non-radiative rate is low under normal operation conditions. The corresponding recombination rate $U^{rad}_{band-band}$ and coefficient B_{rad} can be calculated using the Fermi's golden rule and the transition dipole moment (momentum matrix elements)[63-66].

However, in recent NAMD simulations[21-25,31-35,37-40] an excitation is modelled through a change in occupation numbers of valence and conduction bands of the supercell. Recombination towards the ground state is then simulated by NAMD and the band-to-band recombination lifetime τ is calculated by fitting the decay of the electron population using $P(t) = \exp(-t/\tau)$. These simulations are in the microcanonical (NVE) ensemble, so the electronic energy decrease is converted into vibrational (kinetic) energy through the electron-phonon coupling, which obeys the energy conservation rule. Emission of light is not considered and the associated lifetime is in fact $\tau^{non-rad}_{band-band}$. This was also pointed out by Kim and Walsh[53].

The contribution $\tau^{non-rad}_{band-band}$ is just part of the $\tau_{band-band}$, whereas $\tau_{band-band}$ is just part of the true effective τ, as shown in Eq. (7). Therefore, the meaning of $\tau^{non-rad}_{band-band}$ calculated in the NAMD studies is different from the effective lifetime that can be measured experimentally. Only when the lifetimes for other mechanisms, such as band-to-band radiative $\tau^{rad}_{band-band}$ and defect-assisted non-radiative τ_{SRH}, are longer, can the calculated $\tau^{non-rad}_{band-band}$ be important. Unfortunately, the importance of the band-to-band non-radiative recombination may be overestimated due to the high carrier density in small supercell models, as discussed next.

Dependence of $\tau_{band-band}$ on Density of Non-Equilibrium Carriers.

Eq. (17) shows that $\tau_{band-band}$ (similarly for $\tau_{band-band}^{non-rad}$) depends not only on the density of non-equilibrium carriers $\Delta n(0)$, but also on the density of equilibrium carriers, n_0 and p_0. If the recombination coefficient $B_{non-rad}$ is known, the dependence of $\tau_{band-band}^{non-rad}$ on $\Delta n(0)$, n_0 and p_0 can be directly calculated. An example is given in Fig. 3a and Fig. 3b, where we assume $B_{non-rad}$=2.6×10^{-12} cm^3/s.

Fig. 3a shows the decrease of $\tau_{band-band}^{non-rad}$ as $\Delta n(0)$ increases from 10^{10} cm^{-3} to 10^{20} cm^{-3} for the given n_0 and p_0. Obviously, $\tau_{band-band}^{non-rad}$ can be as long as hundreds of microseconds if $\Delta n(0)$ is on the order of 10^{15} cm^{-3}, while the value decreases quickly to several nanoseconds if $\Delta n(0)$ increases to 10^{20} cm^{-3}. The large difference can be seen more directly in Fig. 3c and 3d, which show the simulated decay of the non-equilibrium carrier density $\Delta n(t)$ for different initial density $\Delta n(0)$ according to $\frac{d\Delta n(t)}{dt} = -U = -U_{band-band}^{non-rad}$. To demonstrate the influence of the initial density $\Delta n(0)$, $\Delta n(0)$ is set to 2.6×10^{20} cm^{-3} in Fig. 3c and 2.6×10^{15} cm^{-3} in Fig. 3d, which has a difference as large as 5 orders of magnitude. As we can see, the decay in Fig. 3c is very fast and it takes only 1-2 ns for $\Delta n(t)$ decaying to $1/e$ of $\Delta n(0)$, consistent with the short $\tau_{band-band}^{non-rad}$=1.5 ns at $\Delta n(0)$=2.6×10^{20} cm^{-3} in Fig. 3a (for n_0=p_0=10^6 cm^{-3}). In contrast, the decay in Fig. 3d is slower and it takes almost 0.1 ms for $\Delta n(t)$ decaying to $1/e$ of $\Delta n(0)$, consistent with the long $\tau_{band-band}^{non-rad}$=0.15 ms according to Eq. (17). The shorter $\tau_{band-band}^{non-rad}$ for higher $\Delta n(0)$ is easy to understand. As shown schematically in Fig. 2c, when $\Delta n(0)$ is high, there are more non-equilibrium electron and hole carriers in the structure, so they have more chances to interact and recombine. In contrast, when $\Delta n(0)$ is low in Fig. 2d, there are fewer chances for them to interact and the recombination rate is reduced.

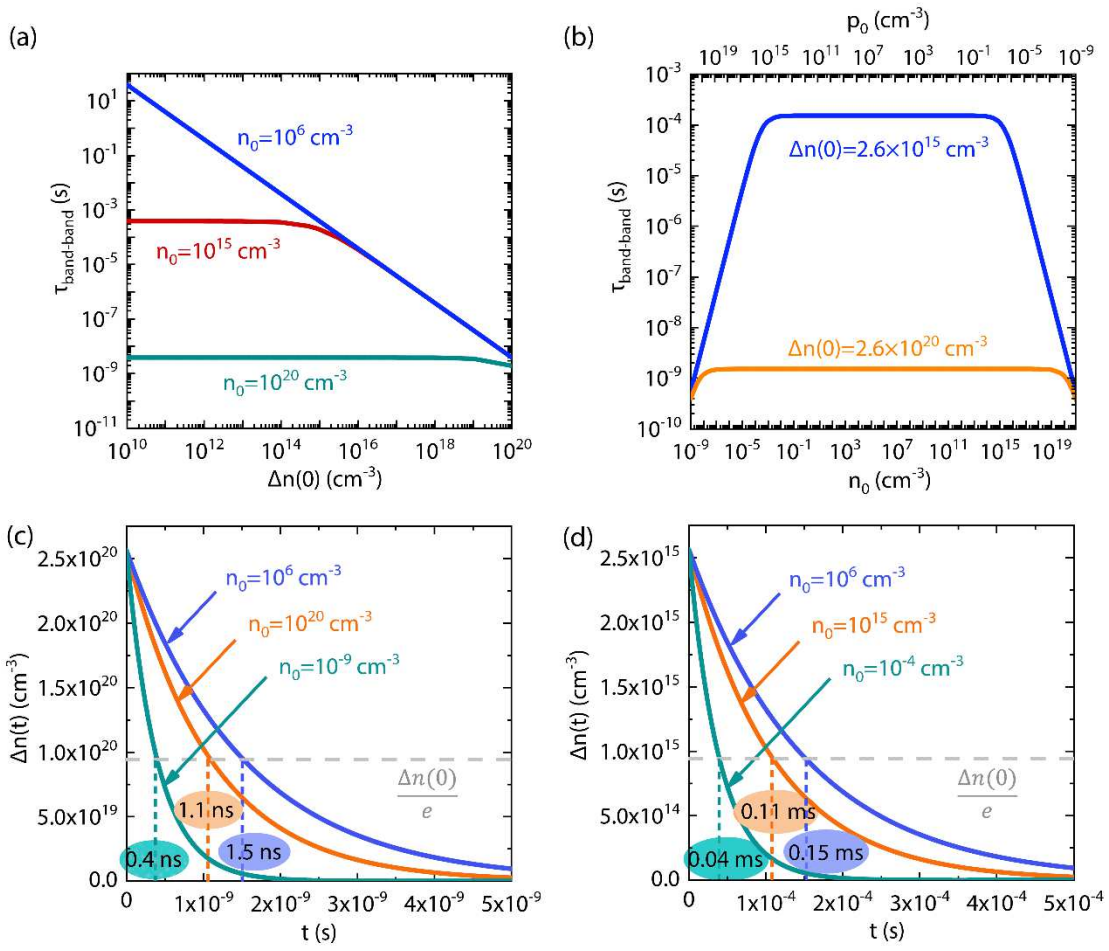

Figure 3. Calculated dependence of $\tau_{band-band}^{non-rad}$ on (a) the density of non-equilibrium carriers $\Delta n(0)$ for the given density of equilibrium carriers n_0 (p_0), and (b) n_0 (p_0) for the given $\Delta n(0)$; and the time evolution of $\Delta n(t)$ for (c) high initial density $\Delta n(0)$=2.6 × 10^{20} cm^{-3} and (d) low $\Delta n(0)$=2.6 × 10^{15} cm^{-3}, when only band-to-band nonradiative recombination is considered. In (c) and (d), three different sets of n_0 (p_0) are considered.

The short $\tau_{band-band}^{non-rad}$ at high $\Delta n(0)$ can be used to explain why the NAMD simulated lifetime is only 1.5 ns in $CH_3NH_3PbI_3$[43], much shorter than the experimental lifetime of several microseconds. As compared in Fig. 2, $\Delta n(0)$ assumed in the NAMD simulations is high (around 10^{20} cm^{-3}), much higher than typical values (around 10^{15} cm^{-3}) in semiconductor samples under one-sun illumination. If instead, the simulation uses a very large supercell with 10^7 atoms, $\Delta n(0)$ decreases to around 10^{15} cm^{-3}, then $\tau_{band-band}^{non-rad}$ can be as long as 10^5 ns, as shown in Fig. 3d. Based on the analysis, the large difference between the recent simulations and experiments for $CH_3NH_3PbI_3$ can

now be understood, *i.e.*, the short lifetime of 1.5 ns from NAMD simulations is not the effective $\tau_{band-band}^{non-rad}$ or the total effective τ in real samples, so it is meaningless to compare the value to the experimental lifetime directly. Only after all the contributions of the effective $\tau_{band-band}^{non-rad}$, $\tau_{band-band}^{rad}$, τ_{SRH} and τ_{Auger} are considered at the actual $\Delta n(0)$ and the total effective τ is calculated, can comparison to measurements be made.

A suitable way to predict the effective $\tau_{band-band}^{non-rad}$ is by adopting Eq. (17) to derive the supercell-size-independent recombination coefficient $B_{non-rad}$ from the raw $\tau_{band-band}^{non-rad}$ derived from the NAMD supercell simulations. Eq. (17) is changed into

$$B_{non-rad} = \frac{1}{\tau_{band-band}^{non-rad}[n_0+p_0+\Delta n(0)]} \qquad (21).$$

The densities of equilibrium carriers, n_0 and p_0, should be small in the defect-free (dopant-free) supercell and can be neglected compared to $\Delta n(0)$, because the band gap is above 1.5 eV and the thermal excitation of carriers can be neglected. As a result, $B_{non-rad} = \frac{1}{\tau_{band-band}^{non-rad} * \Delta n(0)}$.

To take one example, Qiao *et al.* derived a lifetime $\tau_{band-band}^{non-rad}$ of 1.5 ns from the NAMD simulation using a 192-atom $CH_3NH_3PbI_3$ supercell[43], in which $\Delta n(0)$=2.6×10^{20} cm^{-3}. Then the derived $B_{non-rad} \approx 2.6 \times 10^{-12}$ cm^3/s. With the derived $B_{non-rad}$, we can calculate the effective $\tau_{band-band}^{non-rad}$ for low $\Delta n(0)$ according to Eq. (17). For standard $\Delta n(0)$ around 10^{15} cm^{-3} under sunlight illumination, the effective $\tau_{band-band}^{non-rad}$ should be around 150 μs, which is higher than the directly derived value of 1.5 ns by 5 orders of magnitude. As a result, the recombination coefficient $B_{non-rad}$ derived from the NAMD simulations[43] gives a long $\tau_{band-band}^{non-rad}$ when $\Delta n(0)$ is set to a reasonable value. Such a long $\tau_{band-band}^{non-rad}$ is in accordance with longstanding non-radiative carrier capture theories (which stem from Landau-Zener theory that describes the probability of transition following a non-adiabatic level crossing, however, the band gap of $CH_3NH_3PbI_3$ acts as a substantial barrier that prohibits band-to-band non-radiative recombination)[53]. If the effective τ_{SRH} or $\tau_{band-band}^{rad}$ is shorter than 10 μs, the contribution of the long effective $\tau_{band-band}^{non-rad}$ (150 μs) to the total effective τ can be negligible. The comparison of τ_{SRH}, $\tau_{band-band}^{rad}$ and $\tau_{band-band}^{non-rad}$ will be discussed later.

With the approach to determine the effective $\tau_{band-band}^{non-rad}$, we can revisit other NAMD studies which reported carrier lifetimes. Ghosh *et al.* investigated the excited-

state carrier dynamics near the band edges of $(BA)_2PbBr_4$ and $(PEA)_2PbBr_4$ perovskites using the NAMD simulation and the calculated lifetime is 668 ps and 2158 ps, respectively, for $\Delta n(0)=10^{20}$ cm^{-3} in the supercell[31]. Therefore, the corresponding coefficients $B_{non-rad}$ are 1.5×10^{-11} cm^3/s and 4.6×10^{-12} cm^3/s. According to Eq. (17), the effective $\tau_{band-band}^{non-rad}$ should be 66.8 μs and 215.8 μs if the real density of photo-excited carriers is 10^{15} cm^{-3}. Besides, Syzgantseva *et al.* predicted the carrier lifetime of pristine UiO-66-NH_2 to be 37 ns from NAMD simulation[33]. With $\Delta n(0)=10^{20}$ cm^{-3} used in their simulation, the coefficient $B_{non-rad}$ can be calculated as 2.7×10^{-13} cm^3/s. If the real density of photo-excited carriers is 10^{15} cm^{-3}, the effective $\tau_{band-band}^{non-rad}$ should be 3.7 ms instead. As we can see in the two examples, the effective $\tau_{band-band}^{non-rad}$ in the real semiconductors are all very long and much longer than the values derived directly from the NAMD simulations, so it is highly necessary to perform the conversion based on Eqs. (21) and (17) to get the effective $\tau_{band-band}^{non-rad}$. Furthermore, such large values of effective $\tau_{band-band}^{non-rad}$ are consistent it not being a limiting process in determining the total lifetime, so it is necessary to consider other mechanisms and compare $\tau_{band-band}^{rad}$, τ_{SRH} and τ_{Auger} to $\tau_{band-band}^{non-rad}$.

According to Eq. (17), the densities of equilibrium carriers, n_0 and p_0, also influence $\tau_{band-band}$ (similarly for $\tau_{band-band}^{non-rad}$). In Fig. 3a, the dependence of $\tau_{band-band}^{non-rad}$ on $\Delta n(0)$ for three different set of n_0 (p_0) are considered. In Fig. 3b, the dependence of $\tau_{band-band}^{non-rad}$ on n_0 (p_0) are explicitly plotted for low and high $\Delta n(0)$. As we can see, when n_0 and p_0 are both much lower than $\Delta n(0)$, $\tau_{band-band}^{non-rad}$ is almost independent of n_0 and p_0, because Eq. (17) is simplified into $\tau_{band-band}^{non-rad} = \frac{1}{B_{non-rad}\Delta n(0)}$. This is the case for most of intrinsic semiconductors with the Fermi level close to the middle of band gap, whose n_0 and p_0 are usually low (for intrinsic $CH_3NH_3PbI_3$, n_0 and p_0 can be estimated to be around 10^6 cm^{-3}, much lower than the normal $\Delta n(0)$ around 10^{15} cm^{-3} under sunlight). However, when the semiconductors are doped or there are high densities of defects, n_0 and p_0 can be higher and comparable to $\Delta n(0)$. Here they can reduce the lifetime more significantly, as shown by the shifts of lines in Fig. 3a and the decrease of $\tau_{band-band}^{non-rad}$ at the two ends of Fig. 3b. This can also be seen in Fig. 3c and 3d, in which the simulated decay of $\Delta n(t)$ are obviously faster when n_0 is very high or very low (corresponding to very high p_0). In the previous supercell simulations, very large $\Delta n(0)$ was assumed, so n_0 and p_0 were very small compared to $\Delta n(0)$ and their

influences can be neglected. However, the real $\Delta n(0)$ in the working photovoltaic devices is only around 10^{15} cm^{-3}. Doping or intrinsic defects can produce equilibrium carriers with n_0 or p_0 as high as 10^{17} cm^{-3} in $CH_3NH_3PbI_3$[67,68], then the reduction of $\tau_{band-band}^{non-rad}$ caused by n_0 and p_0 can be dramatic. In such cases, it is necessary to consider the influences of n_0 and p_0 when discussing the lifetime of photo-excited carriers.

Dependence of τ_{SRH} on Density of Recombination-Center Defects.

When there are point defects or dopants in a crystal, they not only produce equilibrium carriers (influencing n_0 and p_0), but also induce the SRH non-radiative recombination of non-equilibrium carriers, thus affecting the lifetime. Eqs. (6) and (7) show the contribution of the SRH recombination to the recombination rate (by U_{SRH}) and lifetime (by τ_{SRH}).

In Fig. 4, we simulate the decay of the non-equilibrium carrier density $\Delta n(t)$ according to $\frac{d\Delta n(t)}{dt} = -U_{SRH}$ and Eq. (11) for $CH_3NH_3PbI_3$ containing recombination-center defects. We assume the electron capture coefficient c_n and hole capture coefficient c_p of the defect in Eq. (14) to be 10^{-7} cm^3·s^{-1}, which are the normal carrier capture coefficients of defects in semiconductors[60,69-71]. Then the SRH recombination coefficient A can be derived at a given defect density N_t following Eq. (14). In Fig. 4a and 4b, the simulated decay of carrier density is shown for the cases when n_0=p_0=10^6 cm^{-3}, and the defect density N_t=2.6×10^{20} cm^{-3} (corresponding to the high defect density in the NAMD simulations where a defect is put in a supercell with hundreds of atoms) and $N_t = 10^{15}$ cm^{-3} (corresponding to the common defect or doping density in semiconductors), respectively. The decay is fast for high N_t in Fig. 4a, with a short lifetime τ_{SRH}=7.8×10^{-5} ns. In contrast, τ_{SRH} becomes much longer and increases to 20 ns when N_t is 10^{15} cm^{-3}. The comparison shows clearly that N_t has significant influence on τ_{SRH}, as described by Eqs. (14) and (16), which is easy to understand because a higher density of defects can capture more carriers per unit time.

Considering the dependence of τ_{SRH} on N_t, the derived lifetime from the NAMD simulations[72,73] with one defect in a several-hundred-atom supercell ($N_t \approx 10^{20}$ cm^{-3}) should not be interpreted as a true lifetime. An approach for extracting the SRH lifetime

from the small-supercell NAMD simulations is by converting the value to the N_t-independent electron capture coefficient c_n and hole capture coefficient c_p of the defect according to Eqs. (14) and (16), then the lifetime in real samples with different N_t can be calculated using the same equations.

In another example, Shi *et al.* carried out the simulations of the charge trapping processes in $CH_3NH_3PbBr_3$ containing the DY^- center[72]. The obtained decay time is 1.9 ns for CBM-to-defect trapping and 4.7×10^{-2} ns for VBM-to-defect trapping, respectively. With the defect density (1.8×10^{20} cm^{-3}) in their NAMD simulation, we can extract the electron capture coefficient (c_n) of 2.9×10^{-12} $cm^3 \cdot s^{-1}$ and hole capture coefficient (c_p) of 1.2×10^{-10} $cm^3 \cdot s^{-1}$ according to $\tau_{SRH} = \frac{1}{N_t c_n}$ for electron capture and $\frac{1}{N_t c_p}$ for hole capture. The values are low compared to the normal carrier capture coefficients of defects in semiconductors (10^{-7} $cm^3 \cdot s^{-1}$)[60,69-71]. Assuming N_t in real semiconductors is 10^{15} cm^{-3} and $\Delta n(0)$=10^{15} cm^{-3}, τ_{SRH} is 345 μs according to Eqs. (14) and (16). Therefore, such a defect should not cause serious limit to the lifetime of photo-excited carriers in $MAPbBr_3$ when the densities of the defect and photo-excited carriers are at the medium level.

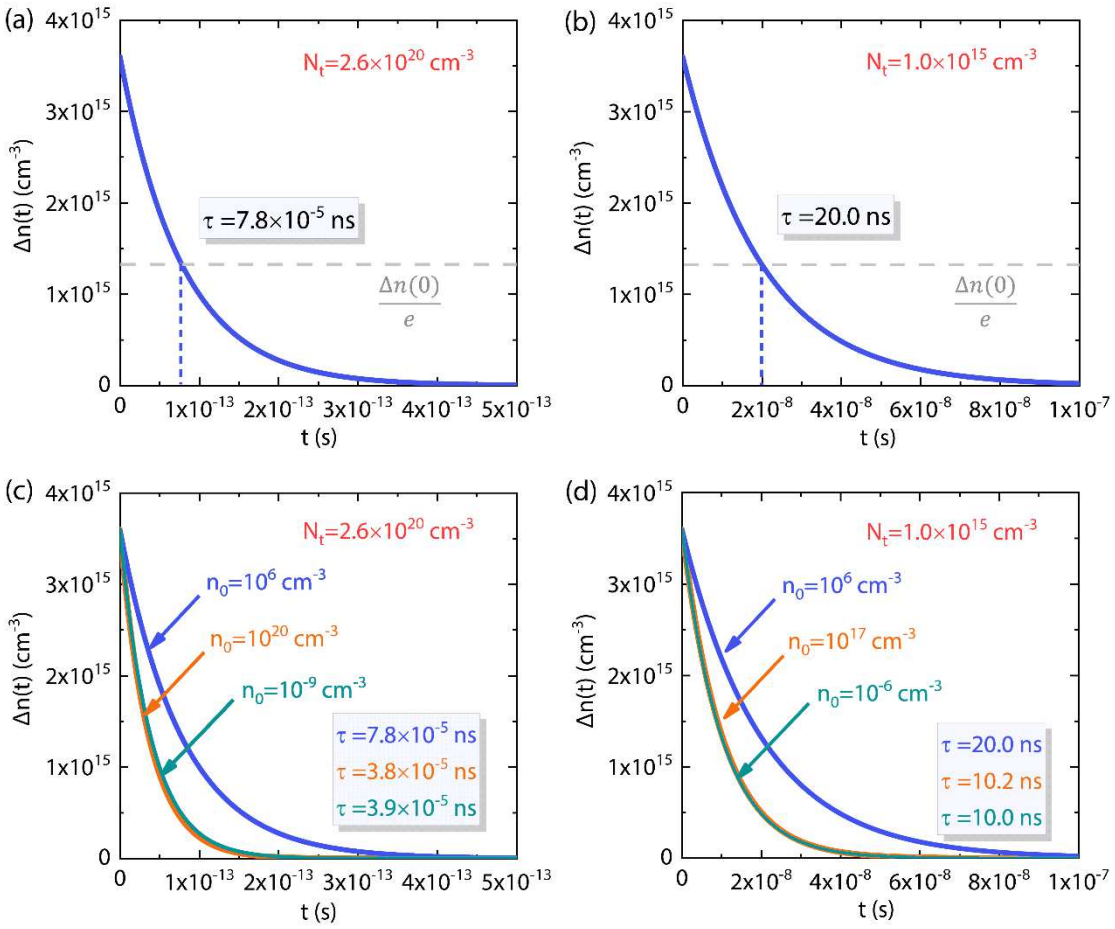

Figure 4. Decay of non-equilibrium carrier density when only the SRH recombination is considered. The non-equilibrium carrier density at t=0 is set to 3.6×10^{15} cm^{-3}. N_t is $2.6 \times 10^{20}\ cm^{-3}$ in (a) and (c) and 1.0×10^{15} cm^{-3} in (b) and (d). The equilibrium carrier density is n_0=p_0=$0.85\times 10^6 \approx 10^6$ cm^{-3} in both (a) and (b). In (c), n_0 varies from 10^{20} to 10^{-9} cm^{-3} (p_0 from 7.3×10^{-9} to 7.3×10^{20} cm^{-3}). In (d), n_0 varies from 10^{17} to 10^{-6} cm^{-3} (p_0 from 7.3×10^{-6} to 7.3×10^{17} cm^{-3}).

In Fig. 4a and 4b, only the influence of N_t is shown while n_0 and p_0 are fixed. However, according to Eqs. (14) and (16), the SRH recombination coefficient A and τ_{SRH} also depend on n_0 and p_0. In Fig. 4c and 4d, the influences of n_0 and p_0 are also simulated. In Fig. 4c different n_0 and p_0 are considered for high N_t=10^{20} cm^{-3}: (i) the sample is highly n-type with a high n_0=10^{20} cm^{-3} and low p_0= 7.3×10^{-9} cm^{-3}, (ii) the sample is intrinsic with low n_0=p_0=10^6 cm^{-3}, and (iii) the sample is highly p-type with a high p_0=7.3×10^{20} cm^{-3} and low n_0=10^{-9} cm^{-3}. The simulation shows that τ_{SRH} becomes shorter in the highly n-type or p-type samples, so the increase of the

equilibrium carrier densities can facilitate the recombination. However, the values are still on the same order of magnitude, so the change is small despite the large changes in n_0 and p_0. When N_t is not very high (10^{15} cm^{-3}), the simulation in Fig. 4d also shows that the change of n_0 or p_0 by 10^{17} cm^{-3} induces only small changes in τ_{SRH}, from around 20 ns to 10 ns. From Figs. 4c and 4d, we can see that τ_{SRH} is mainly determined by N_t, and the influences of n_0 and p_0 are small. This can be understood according to Eq. (14) in which n_0 and p_0 are present in both the numerator and denominator, so their changes are cancelled largely, giving rise to small influences on the recombination coefficient A and the lifetime τ_{SRH}.

Comparison of Different Recombination Mechanisms in $CH_3NH_3PbI_3$.

The effective lifetime τ of non-equilibrium carriers is influenced by all recombination mechanisms. Our analysis has shown that τ_{SRH}, $\tau_{band-band}^{non-rad}$, $\tau_{band-band}^{rad}$ and τ_{Auger} depend on the density of non-equilibrium carriers $\Delta n(0)$, the density of equilibrium carriers n_0 and p_0, and the density of recombination-center defects N_t. When calculating τ, these quantities should be obtained as summarized by the calculation procedure in Fig. 1b. For a semiconductor sample, the density of recombination-center defect or dopant (N_t) and the density of the equilibrium carriers (n_0 and p_0) are usually fixed by the synthesis or annealing conditions. However, the density of non-equilibrium carriers $\Delta n(0)$ in the real samples depends on the environment, *e.g.*, the intensity of the light illumination. To calculate the total effective lifetime τ, *e.g.*, in $CH_3NH_3PbI_3$ samples, we will first show how to calculate $\Delta n(0)$ under illumination.

In the dark, the density of non-equilibrium carriers is 0. If the above bandgap illumination starts at t = 0, the density $\Delta n(t)$ increases with the rate $\frac{d\Delta n(t)}{dt}$ given by Eq. (1). After a certain time, the system will reach a steady state because the carrier generation and recombination is balanced, and the carrier density $\Delta n(t)$ will maintain at a steady value, as given by

$$\frac{d\Delta n(t)}{dt} = G(t) - U(t) = 0 \quad (22).$$

In Fig. 5a, we simulate the increasing process of $\Delta n(t)$ in the $CH_3NH_3PbI_3$ thin film.

For the solar illumination on thin films with a layer thickness *d*, the generation rate *G(t)* of non-equilibrium carriers is a constant and can be calculated as[51],

$$G(t) = (hc)^{-1} \int f_{solar}(\lambda)\alpha(\lambda) \exp(-\alpha(\lambda)d)\, \lambda d\lambda \qquad (23)$$

where *d* is the film thickness of the absorption layer, *h* is the Planck constant, *c* is the speed of light, $f_{solar}(\lambda)$ is the ASTM G173-03 Global Tilt reference spectrum for the solar spectral irradiance distribution, $\alpha(\lambda)$ is the absorbance spectrum of the semiconductor and λ is the wavelength of the light. Using the absorption spectrum taken from Ref. [74], the calculated generation rate *G* is 1.3×10^{21} cm^{-3}·s^{-1} for the 300 nm thick film. The recombination rate *U(t)* can be calculated using,

$$U = U_{SRH} + U_{band-band} + U_{Auger}$$

$$= A \cdot \Delta n(t) + (B_{rad} + B_{non-rad}) \cdot [n_0 + p_0 + \Delta n(t)] \cdot \Delta n(t) + C \cdot \Delta n(t)^3 \qquad (24),$$

in which the SRH, band-to-band (radiative and non-radiative) recombination and Auger recombination are all considered. The SRH recombination coefficient *A* is calculated assuming the density of recombination-center defect has two representative values N_t= 10^{15} and 10^8 cm^{-3}, electron capture coefficient and hole capture coefficient $c_n = c_p = 10^{-7}$ cm^3·s^{-1} (normal carrier capture coefficients of defects in semiconductors[60,69-71]) and n_0= p_0= 0.85×10^6 cm^{-3}. The band-to-band radiative recombination coefficient B_{rad}= 1.1×10^{-10} cm^3/s in $CH_3NH_3PbI_3$ had been calculated by Zhang *et al.*[64]. The band-to-band non-radiative recombination coefficient $B_{non-rad}$= 2.6×10^{-12} cm^3/s had been derived above based on the NAMD simulation of Qiao *et al.*[43]. With *G* and *U*, $\Delta n(t)$ as a function of *t* can be simulated, as shown in Fig. 5a.

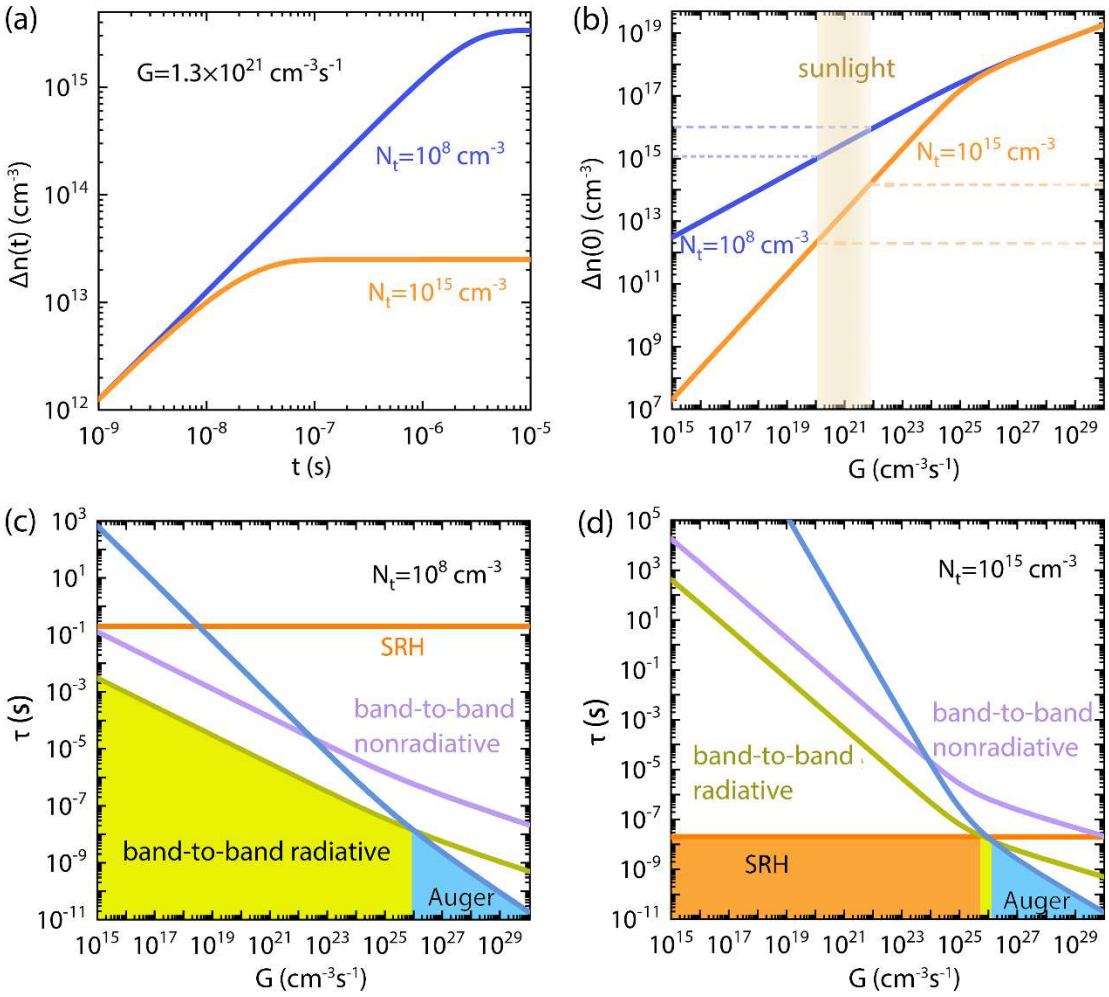

At t=0, $\Delta n(t)$ is 0, then it starts to increase under the light illumination. As t increases, the system finally reaches the steady state and $\Delta n(t)$ plateaus. As shown in Fig. 5a, $\Delta n(t)$ reaches a steady value of $2.5 \times 10^{13}\ cm^{-3}$ at $t \approx 10^{-7}$ s when N_t=$10^{15}\ cm^{-3}$, while it reaches a steady value of $3.3 \times 10^{15}\ cm^{-3}$ at $t \approx 10^{-5}$ s for $N_t = 10^{8}\ cm^{-3}$. Therefore, the steady density of non-equilibrium carriers and the time

taken to reach steady state are sensitive to the defect density. A higher defect density facilitates SRH recombination and thus decreases the time to reach the steady state. In Fig. 5b, we also simulated the steady density of non-equilibrium carriers for varied generation rate *G*, which corresponds to different illumination intensity. When *G* is below 10^{26} cm^{-3}·s^{-1}, the steady-state density increases almost linearly as *G* increases. The generation rate under the sunlight illumination is shown by the shaded area, and the steady density is around 10^{13} cm^{-3} for $N_t = 10^{15}$ cm^{-3} and 10^{15} cm^{-3} for $N_t = 10^{8}$ cm^{-3}, which are much lower than the density of non-equilibrium carriers (around 10^{20} cm^{-3}) in small supercells. Only under concentrated light of 10^5 suns, can the values reach 10^{20} cm^{-3}.

For a $CH_3NH_3PbI_3$ thin film with given N_t, E_t, c_n, c_p, n_0 and p_0, the steady density of non-equilibrium carriers under the sunlight illumination should be taken as $\Delta n(0)$ when calculating the lifetime of non-equilibrium carriers in solar cells. Since the steady-state density changes with the generation rate *G*, the lifetime should also change with *G*. When $\Delta n(0)$, N_t, E_t, c_n, c_p, n_0, p_0, B_{rad} and $B_{non-rad}$ are known, τ_{SRH}, $\tau_{band-band}^{rad}$, $\tau_{band-band}^{non-rad}$ and τ_{Auger} can be calculated directly, as shown in Fig. 1b. Figs. 5c and 5d show how *G* influences the calculated τ_{SRH}, $\tau_{band-band}^{rad}$, $\tau_{band-band}^{non-rad}$ and τ_{Auger}.

In Fig. 5c, the density of recombination-center defects N_t is set at a low level N_t= 10^8 cm^{-3}, because most of the deep-level defects in $CH_3NH_3PbI_3$ have high formation energies and thus low densities[75-79]. The results showed that τ_{SRH} is always around 0.1 s, which is almost independent of *G* because the influences of $\Delta n(0)$ on the SRH recombination coefficient A are cancelled partially in the numerator and denominator of Eq. (14). In contrast, $\tau_{band-band}^{rad}$ and $\tau_{band-band}^{non-rad}$ are sensitive to *G* and decrease quickly as the light intensity and *G* increase, because the band-to-band radiative and non-radiative recombination coefficients B_{rad} and $B_{non-rad}$ depend on $\Delta n(0)$ almost linearly and thus also on *G*. Comparing τ_{SRH}, $\tau_{band-band}^{rad}$, $\tau_{band-band}^{non-rad}$ and τ_{Auger}, band-to-band radiative recombination is the fastest recombination mechanism and determines the total effective τ when *G* is lower than 10^{26} cm^{-3}·s^{-1}, and the Auger recombination dominates at very high generation rates (corresponding to high carrier densities). In contrast, the SRH and band-to-band non-radiative mechanisms only cause slower recombination and thus just decrease τ slightly according to Eqs. (7) and (20).

For one-sun illumination, G is around 10^{21} $cm^{-3}\cdot s^{-1}$, and the steady-state density of non-equilibrium carriers is around 10^{15} cm^{-3}, so the total effective lifetime $\tau \approx \tau_{band-band}^{rad} \approx 1$ μs. The dominance of the band-to-band radiative recombination and the predicted long effective lifetime τ are consistent with the experimental finding of efficient photoluminescence and measured long carrier lifetime around 1 μs in the $CH_3NH_3PbI_3$ thin films[80].

If the density of recombination-center defects N_t is increased, the dominant recombination mechanism can be changed. Fig. 5d shows the case for higher $N_t = 10^{15}$ cm^{-3}, which is common for the deep-level defects in many semiconductors. τ_{SRH} is now shorter, around 10 ns. The SRH recombination determines the total effective lifetime τ when the light intensity is low and G is lower than 10^{25} $cm^{-3}\cdot s^{-1}$, while the band-to-band radiative recombination determines τ only in a small range of G around 10^{26} $cm^{-3}\cdot s^{-1}$. When the light intensity is high and G is higher, Auger recombination becomes dominant. Therefore, there is a transition of the dominant recombination mechanism as the light intensity and G increase. For the sunlight illumination, the steady-state density of non-equilibrium carriers is around 10^{13} cm^{-3} (Fig. 5b), so SRH recombination is dominant.

Our analysis confirms that the lifetime of non-equilibrium carriers in $CH_3NH_3PbI_3$ solar cells should be mainly determined by the band-to-band radiative recombination and is usually very long. Only when thin films have high density of recombination-center defects or dopants, can SRH recombination appreciably decrease the lifetime. Across whole range of G, $\tau_{band-band}^{non-rad}$ is always longer than $\tau_{band-band}^{rad}$ by two orders of magnitude, so the influence of band-to-band non-radiative recombination on the effective τ is negligible in the $CH_3NH_3PbI_3$ thin films, no matter under strong or weak light illumination. Therefore, changes in $\tau_{band-band}^{non-rad}$ alone should not be overinterpreted, *e.g.*, 1.5 ns for the pristine $CH_3NH_3PbI_3$ compared to 4-11 ns for doped or defective crystals[43]. The experimentally improved performance of $CH_3NH_3PbI_3$ solar cells after the alkaline metal treatments should result from the significantly increased τ_{SRH}, because the alkaline metal dopants passivate the recombination-center level of the I interstitial and thus give a clean band gap.

Concluding Remarks

This study is motivated by the development of more quantitative predictions of carrier recombination processes and the lifetimes of non-equilibrium carriers in semiconductors. From the recent literature, there is a striking discrepancy between the carrier lifetimes derived directly from the NAMD simulations using small supercells under periodic boundary conditions and the experimentally measured carrier lifetimes.

By revisiting the fundamental definition of carrier lifetime and considering four recombination mechanisms, we were able to develop a systematic procedure for calculating the effective lifetime of non-equilibrium carriers in semiconductors. Within this procedure, the NAMD and other methods are combined to calculate the effective lifetime that can be compared directly to the experimental values. The calculated results reinforce fundamental concepts in the field, and demonstrate that two factors have significant influence on calculated lifetimes: (i) the consideration of radiative and non-radiative recombination mechanisms, and (ii) the density of equilibrium carriers, non-equilibrium carriers, and recombination-center defects. Recent calculations of carrier lifetimes in $CH_3NH_3PbI_3$ and other optoelectronic semiconductors were limited by (i) the neglect of band-to-band radiative recombination, and (ii) an exaggerated density of non-equilibrium carriers and defects due to the small supercells, which cause the obvious discrepancies between calculations and experiments. Using our procedure, these discrepancies are overcome and the calculated effective lifetime of $CH_3NH_3PbI_3$ can agree well with experiments. Furthermore, our analysis revealed that the effective lifetime is determined by band-to-band radiative and defect-assisted non-radiative recombination, rather than the band-to-band non-radiative recombination ($\tau_{band-band}^{non-rad}$) whose influence is always negligible. Previous conclusions based on the interpretation of changes in $\tau_{band-band}^{non-rad}$ should be revisited. These results demonstrate that it is possible to calculate the carrier lifetime in agreement with experimentally measured values based on the NAMD simulations. The systematic procedure reported here can enable more accurate future studies of carrier dynamics in semiconductors.

Acknowledgements

This work was supported by Shanghai Academic/Technology Research Leader (19XD1421300), National Natural Science Foundation of China (NSFC) under grant Nos. 12174060, 11991060, 12088101 and U1930402, Program for Professor of Special Appointment (Eastern Scholar TP2019019), National Key Research and Development Program of China (2019YFE0118100), State Key Laboratory of ASIC & System (2021MS006) and Young Scientist Project of MOE Innovation Platform. X. G. was supported by NSFC under grant No. 12188101.

References

1 Feldmann, S., Macpherson, S., Senanayak, S. P., Abdi-Jalebi, M., Rivett, J. P. H., Nan, G., Tainter, G. D., Doherty, T. A. S., Frohna, K., Ringe, E., Friend, R. H., Sirringhaus, H., Saliba, M., Beljonne, D., Stranks, S. D. & Deschler, F. Photodoping through local charge carrier accumulation in alloyed hybrid perovskites for highly efficient luminescence. *Nature Photonics* **14**, 123-128 (2020).

2 Christians, J. A., Miranda Herrera, P. A. & Kamat, P. V. Transformation of the Excited State and Photovoltaic Efficiency of $CH_3NH_3PbI_3$ Perovskite upon Controlled Exposure to Humidified Air. *Journal of the American Chemical Society* **137**, 1530-1538 (2015).

3 Niu, X., Bai, X., Zhou, Z. & Wang, J. Rational Design and Characterization of Direct Z-Scheme Photocatalyst for Overall Water Splitting from Excited State Dynamics Simulations. *ACS Catalysis* **10**, 1976-1983 (2020).

4 Shen, L., Fang, Y., Wang, D., Bai, Y., Deng, Y., Wang, M., Lu, Y. & Huang, J. A Self-Powered, Sub-nanosecond-Response Solution-Processed Hybrid Perovskite Photodetector for Time-Resolved Photoluminescence-Lifetime Detection. *Advanced Materials* **28**, 10794-10800 (2016).

5 Guo, Z., Wan, Y., Yang, M., Snaider, J., Zhu, K. & Huang, L. Long-range hot-carrier transport in hybrid perovskites visualized by ultrafast microscopy. *Science* **356**, 59-62 (2017).

6 Liu, X., Kang, F., Hu, C., Wang, L., Xu, Z., Zheng, D., Gong, W., Lu, Y., Ma, Y. & Wang, J. A genetically encoded photosensitizer protein facilitates the rational design of a miniature photocatalytic CO_2-reducing enzyme. *Nature Chemistry* **10**, 1201-1206 (2018).

7 Zheng, Q., Chu, W., Zhao, C., Zhang, L., Guo, H., Wang, Y., Jiang, X. & Zhao, J. Ab initio nonadiabatic molecular dynamics investigations on the excited carriers in condensed matter systems. *WIREs Computational Molecular Science* **9**, e1411 (2019).

8 Curchod, B. F. E. & Martínez, T. J. Ab Initio Nonadiabatic Quantum Molecular Dynamics. *Chemical Reviews* **118**, 3305-3336 (2018).

9 Runge, E. & Gross, E. K. U. Density-Functional Theory for Time-Dependent Systems. *Physical Review Letters* **52**, 997-1000 (1984).

10 Chu, W., Zheng, Q., Prezhdo Oleg, V., Zhao, J. & Saidi Wissam, A. Low-frequency lattice phonons in halide perovskites explain high defect tolerance toward electron-hole recombination. *Science Advances* **6**, eaaw7453 (2020).

11 Chu, W., Zheng, Q., Prezhdo, O. V. & Zhao, J. CO_2 Photoreduction on Metal Oxide Surface Is

Driven by Transient Capture of Hot Electrons: Ab Initio Quantum Dynamics Simulation. *Journal of the American Chemical Society* **142**, 3214-3221 (2020).

12 Akimov, A. V. & Prezhdo, O. V. The PYXAID Program for Non-Adiabatic Molecular Dynamics in Condensed Matter Systems. *Journal of Chemical Theory and Computation* **9**, 4959-4972 (2013).

13 Pal, S., Trivedi, D. J., Akimov, A. V., Aradi, B., Frauenheim, T. & Prezhdo, O. V. Nonadiabatic Molecular Dynamics for Thousand Atom Systems: A Tight-Binding Approach toward PYXAID. *Journal of Chemical Theory and Computation* **12**, 1436-1448 (2016).

14 Lian, C., Hu, S.-Q., Zhang, J., Cheng, C., Yuan, Z., Gao, S. & Meng, S. Integrated Plasmonics: Broadband Dirac Plasmons in Borophene. *Physical Review Letters* **125**, 116802 (2020).

15 Hong, H., Zhang, J., Zhang, J., Qiao, R., Yao, F., Cheng, Y., Wu, C., Lin, L., Jia, K., Zhao, Y., Zhao, Q., Gao, P., Xiong, J., Shi, K., Yu, D., Liu, Z., Meng, S., Peng, H. & Liu, K. Ultrafast Broadband Charge Collection from Clean Graphene/$CH_3NH_3PbI_3$ Interface. *Journal of the American Chemical Society* **140**, 14952-14957 (2018).

16 Zhou, Z., Niu, X., Zhang, Y. & Wang, J. Janus MoSSe/WSeTe heterostructures: a direct Z-scheme photocatalyst for hydrogen evolution. *Journal of Materials Chemistry A* **7**, 21835-21842 (2019).

17 Long, C., Dai, Y., Gong, Z.-R. & Jin, H. Robust type-II band alignment in Janus-MoSSe bilayer with extremely long carrier lifetime induced by the intrinsic electric field. *Physical Review B* **99**, 115316 (2019).

18 Wang, J., Li, W. & Yin, W.-J. Passivating Detrimental DX Centers in $CH_3NH_3PbI_3$ for Reducing Nonradiative Recombination and Elongating Carrier Lifetime. *Advanced Materials* **32**, 1906115 (2020).

19 Crespo-Otero, R. & Barbatti, M. Recent Advances and Perspectives on Nonadiabatic Mixed Quantum–Classical Dynamics. *Chemical Reviews* **118**, 7026-7068 (2018).

20 Pan, J. Computationally probing exciton dynamics. *Nature Computational Science* **1**, 246-246 (2021).

21 He, J., Fang, W.-H., Long, R. & Prezhdo, O. V. Why Oxygen Increases Carrier Lifetimes but Accelerates Degradation of $CH_3NH_3PbI_3$ under Light Irradiation: Time-Domain Ab Initio Analysis. *Journal of the American Chemical Society* **142**, 14664-14673 (2020).

22 Li, W., Sun, Y.-Y., Li, L., Zhou, Z., Tang, J. & Prezhdo, O. V. Control of Charge Recombination in Perovskites by Oxidation State of Halide Vacancy. *Journal of the American Chemical Society* **140**, 15753-15763 (2018).

23 Ghosh, D., Acharya, D., Pedesseau, L., Katan, C., Even, J., Tretiak, S. & Neukirch, A. J. Charge carrier dynamics in two-dimensional hybrid perovskites: Dion–Jacobson vs. Ruddlesden–Popper phases. *Journal of Materials Chemistry A* **8**, 22009-22022 (2020).

24 He, J., Fang, W.-H. & Long, R. Unravelling the effects of oxidation state of interstitial iodine and oxygen passivation on charge trapping and recombination in $CH_3NH_3PbI_3$ perovskite: a time-domain ab initio study. *Chemical Science* **10**, 10079-10088 (2019).

25 Kim, T. W., Jun, S., Ha, Y., Yadav, R. K., Kumar, A., Yoo, C.-Y., Oh, I., Lim, H.-K., Shin, J. W., Ryoo, R., Kim, H., Kim, J., Baeg, J.-O. & Ihee, H. Ultrafast charge transfer coupled with lattice phonons in two-dimensional covalent organic frameworks. *Nature Communications* **10**, 1873 (2019).

26 Mai, S., Pollum, M., Martínez-Fernández, L., Dunn, N., Marquetand, P., Corral, I., Crespo-

Hernández, C. E. & González, L. The origin of efficient triplet state population in sulfur-substituted nucleobases. *Nature Communications* **7**, 13077 (2016).

27 Du, L. & Lan, Z. An On-the-Fly Surface-Hopping Program JADE for Nonadiabatic Molecular Dynamics of Polyatomic Systems: Implementation and Applications. *Journal of Chemical Theory and Computation* **11**, 1360-1374 (2015).

28 Wiebeler, C., Plasser, F., Hedley, G. J., Ruseckas, A., Samuel, I. D. W. & Schumacher, S. Ultrafast Electronic Energy Transfer in an Orthogonal Molecular Dyad. *The Journal of Physical Chemistry Letters* **8**, 1086-1092 (2017).

29 Habib, M., Kar, M., Pal, S. & Sarkar, P. Role of Chalcogens in the Exciton Relaxation Dynamics of Chalcogenol-Functionalized CdSe QD: A Time-Domain Atomistic Simulation. *Chemistry of Materials* **31**, 4042-4050 (2019).

30 Zhang, Y., Li, L., Tretiak, S. & Nelson, T. Nonadiabatic Excited-State Molecular Dynamics for Open-Shell Systems. *Journal of Chemical Theory and Computation* **16**, 2053-2064 (2020).

31 Ghosh, D., Neukirch, A. J. & Tretiak, S. Optoelectronic Properties of Two-Dimensional Bromide Perovskites: Influences of Spacer Cations. *The Journal of Physical Chemistry Letters* **11**, 2955-2964 (2020).

32 Xie, X.-Y., Liu, X.-Y., Fang, Q., Fang, W.-H. & Cui, G. Photoinduced Carrier Dynamics at the Interface of Pentacene and Molybdenum Disulfide. *The Journal of Physical Chemistry A* **123**, 7693-7703 (2019).

33 Syzgantseva, M. A., Stepanov, N. F. & Syzgantseva, O. A. Carrier Lifetimes and Recombination Pathways in Metal–Organic Frameworks. *The Journal of Physical Chemistry Letters* **10**, 5041-5046 (2019).

34 Nam, Y., Li, H. & Lee, J. Y. Site-dependent photoinduced charge carrier dynamics in nitrogen/fluorine doped TiO_2 nanoparticles. *Journal of Materials Chemistry C* **9**, 1992-2000 (2021).

35 Li, L. & Carter, E. A. Defect-Mediated Charge-Carrier Trapping and Nonradiative Recombination in WSe_2 Monolayers. *Journal of the American Chemical Society* **141**, 10451-10461 (2019).

36 Yin, J., Maity, P., De Bastiani, M., Dursun, I., Bakr Osman, M., Brédas, J.-L. & Mohammed Omar, F. Molecular behavior of zero-dimensional perovskites. *Science Advances* **3**, e1701793 (2017).

37 Zhang, Z., Fang, W.-H., Long, R. & Prezhdo, O. V. Exciton Dissociation and Suppressed Charge Recombination at 2D Perovskite Edges: Key Roles of Unsaturated Halide Bonds and Thermal Disorder. *Journal of the American Chemical Society* **141**, 15557-15566 (2019).

38 Nijamudheen, A. & Akimov, A. V. Criticality of Symmetry in Rational Design of Chalcogenide Perovskites. *The Journal of Physical Chemistry Letters* **9**, 248-257 (2018).

39 Long, R., Liu, J. & Prezhdo, O. V. Unravelling the Effects of Grain Boundary and Chemical Doping on Electron–Hole Recombination in $CH_3NH_3PbI_3$ Perovskite by Time-Domain Atomistic Simulation. *Journal of the American Chemical Society* **138**, 3884-3890 (2016).

40 Jian, W., Jia, R., Zhang, H.-X. & Bai, F.-Q. Arranging strategies for A-site cations: impact on the stability and carrier migration of hybrid perovskite materials. *Inorganic Chemistry Frontiers* **7**, 1741-1749 (2020).

41 Mai, S., Marquetand, P. & González, L. Non-adiabatic and intersystem crossing dynamics in SO_2. II. The role of triplet states in the bound state dynamics studied by surface-hopping

simulations. *The Journal of Chemical Physics* **140**, 204302 (2014).

42 Song, H., Fischer, S. A., Zhang, Y., Cramer, C. J., Mukamel, S., Govind, N. & Tretiak, S. First Principles Nonadiabatic Excited-State Molecular Dynamics in NWChem. *Journal of Chemical Theory and Computation* **16**, 6418-6427 (2020).

43 Qiao, L., Fang, W.-H., Long, R. & Prezhdo, O. V. Extending Carrier Lifetimes in Lead Halide Perovskites with Alkali Metals by Passivating and Eliminating Halide Interstitial Defects. *Angewandte Chemie International Edition* **59**, 4684-4690 (2020).

44 He, J., Fang, W.-H. & Long, R. Two-Dimensional Perovskite Capping Layer Simultaneously Improves the Charge Carriers' Lifetime and Stability of $MAPbI_3$ Perovskite: A Time-Domain Ab Initio Study. *The Journal of Physical Chemistry Letters* **11**, 5100-5107 (2020).

45 He, J., Fang, W.-H., Long, R. & Prezhdo, O. V. Increased Lattice Stiffness Suppresses Nonradiative Charge Recombination in $MAPbI_3$ Doped with Larger Cations: Time-Domain Ab Initio Analysis. *ACS Energy Letters* **3**, 2070-2076 (2018).

46 Huang, Y., Qiao, L., Jiang, Y., He, T., Long, R., Yang, F., Wang, L., Lei, X., Yuan, M. & Chen, J. A-site Cation Engineering for Highly Efficient $MAPbI_3$ Single-Crystal X-ray Detector. *Angewandte Chemie International Edition* **58**, 17834-17842 (2019).

47 Qiao, L., Fang, W.-H., Long, R. & Prezhdo, O. V. Atomic Model for Alkali Metal Passivation of Point Defects at Perovskite Grain Boundaries. *ACS Energy Letters* **5**, 3813-3820 (2020).

48 Dong, Q., Fang, Y., Shao, Y., Mulligan, P., Qiu, J., Cao, L. & Huang, J. Electron-hole diffusion lengths > 175 μm in solution-grown $CH_3NH_3PbI_3$ single crystals. *Science* **347**, 967-970 (2015).

49 Saidaminov, M. I., Abdelhady, A. L., Murali, B., Alarousu, E., Burlakov, V. M., Peng, W., Dursun, I., Wang, L., He, Y., Maculan, G., Goriely, A., Wu, T., Mohammed, O. F. & Bakr, O. M. High-quality bulk hybrid perovskite single crystals within minutes by inverse temperature crystallization. *Nature Communications* **6**, 7586 (2015).

50 Yamada, Y., Nakamura, T., Endo, M., Wakamiya, A. & Kanemitsu, Y. Photocarrier Recombination Dynamics in Perovskite $CH_3NH_3PbI_3$ for Solar Cell Applications. *Journal of the American Chemical Society* **136**, 11610-11613 (2014).

51 Johnston, M. B. & Herz, L. M. Hybrid Perovskites for Photovoltaics: Charge-Carrier Recombination, Diffusion, and Radiative Efficiencies. *Accounts of Chemical Research* **49**, 146-154 (2016).

52 Richter, J. M., Abdi-Jalebi, M., Sadhanala, A., Tabachnyk, M., Rivett, J. P. H., Pazos-Outón, L. M., Gödel, K. C., Price, M., Deschler, F. & Friend, R. H. Enhancing photoluminescence yields in lead halide perovskites by photon recycling and light out-coupling. *Nature Communications* **7**, 13941 (2016).

53 Kim, S. & Walsh, A. Comment on" Low-frequency lattice phonons in halide perovskites explain high defect tolerance toward electron-hole recombination". *arXiv preprint arXiv:2003.05394* (2020).

54 Chu, W., Zheng, Q., Prezhdo, O. V., Zhao, J. & Saidi, W. A. Response to Comment on" Low-frequency lattice phonons in halide perovskites explain high defect tolerance toward electron-hole recombination". *arXiv preprint arXiv:2004.12559* (2020).

55 Grundmann, M. *Physics of semiconductors*. Vol. 11 (Springer, 2010).

56 Shockley, W. & Read, W. T. Statistics of the Recombinations of Holes and Electrons. *Physical Review* **87**, 835-842 (1952).

57 Hall, R. N. Electron-Hole Recombination in Germanium. *Physical Review* **87**, 387-387 (1952).

58 Hall, R. Recombination processes in semiconductors. *Proceedings of the IEE-Part B: Electronic and Communication Engineering* **106**, 923-931 (1959).

59 Zhang, X., Shen, J.-X. & Van de Walle, C. G. First-Principles Simulation of Carrier Recombination Mechanisms in Halide Perovskites. *Advanced Energy Materials* **10**, 1902830 (2020).

60 Alkauskas, A., Yan, Q. & Van de Walle, C. G. First-principles theory of nonradiative carrier capture via multiphonon emission. *Physical Review B* **90**, 075202 (2014).

61 Shi, L., Xu, K. & Wang, L.-W. Comparative study of ab initio nonradiative recombination rate calculations under different formalisms. *Physical Review B* **91**, 205315 (2015).

62 Shen, J.-X., Zhang, X., Das, S., Kioupakis, E. & Van de Walle, C. G. Unexpectedly Strong Auger Recombination in Halide Perovskites. *Advanced Energy Materials* **8**, 1801027 (2018).

63 Landsberg, P. T. *Recombination in semiconductors*. (Cambridge University Press: Cambridge, 2003).

64 Zhang, X., Shen, J.-X., Wang, W. & Van de Walle, C. G. First-Principles Analysis of Radiative Recombination in Lead-Halide Perovskites. *ACS Energy Letters* **3**, 2329-2334 (2018).

65 Zhang, L., Vasenko, A. S., Zhao, J. & Prezhdo, O. V. Mono-Elemental Properties of 2D Black Phosphorus Ensure Extended Charge Carrier Lifetimes under Oxidation: Time-Domain Ab Initio Analysis. *The Journal of Physical Chemistry Letters* **10**, 1083-1091 (2019).

66 Dreyer, C. E., Alkauskas, A., Lyons, J. L. & Van de Walle, C. G. Radiative capture rates at deep defects from electronic structure calculations. *Physical Review B* **102**, 085305 (2020).

67 Perry, E. E., Labram, J. G., Venkatesan, N. R., Nakayama, H. & Chabinyc, M. L. N-Type Surface Doping of $MAPbI_3$ via Charge Transfer from Small Molecules. *Advanced Electronic Materials* **4**, 1800087 (2018).

68 Wang, Q., Shao, Y., Xie, H., Lyu, L., Liu, X., Gao, Y. & Huang, J. Qualifying composition dependent p and n self-doping in $CH_3NH_3PbI_3$. *Applied Physics Letters* **105**, 163508 (2014).

69 Yablonovitch, E., Bhat, R., Harbison, J. P. & Logan, R. A. Survey of defect-mediated recombination lifetimes in GaAs epilayers grown by different methods. *Applied Physics Letters* **50**, 1197-1199 (1987).

70 Li, J., Yuan, Z.-K., Chen, S., Gong, X.-G. & Wei, S.-H. Effective and Noneffective Recombination Center Defects in Cu_2ZnSnS_4: Significant Difference in Carrier Capture Cross Sections. *Chemistry of Materials* **31**, 826-833 (2019).

71 Zhang, X., Turiansky, M. E., Shen, J.-X. & Van de Walle, C. G. Iodine interstitials as a cause of nonradiative recombination in hybrid perovskites. *Physical Review B* **101**, 140101 (2020).

72 Shi, R., Fang, W.-H., Vasenko, A. S., Long, R. & Prezhdo, O. V. Efficient passivation of DY center in $CH_3NH_3PbBr_3$ by chlorine: Quantum molecular dynamics. *Nano Research* (2021).

73 Qiao, L., Fang, W.-H., Long, R. & Prezhdo, O. V. Elimination of Charge Recombination Centers in Metal Halide Perovskites by Strain. *Journal of the American Chemical Society* **143**, 9982-9990 (2021).

74 Xing, G., Mathews, N., Sun, S., Lim Swee, S., Lam Yeng, M., Grätzel, M., Mhaisalkar, S. & Sum Tze, C. Long-Range Balanced Electron- and Hole-Transport Lengths in Organic-Inorganic $CH_3NH_3PbI_3$. *Science* **342**, 344-347 (2013).

75 Yin, W.-J., Shi, T. & Yan, Y. Unusual defect physics in $CH_3NH_3PbI_3$ perovskite solar cell absorber. *Applied Physics Letters* **104**, 063903 (2014).

76 Adinolfi, V., Yuan, M., Comin, R., Thibau, E. S., Shi, D., Saidaminov, M. I., Kanjanaboos, P.,

Kopilovic, D., Hoogland, S., Lu, Z.-H., Bakr, O. M. & Sargent, E. H. The In-Gap Electronic State Spectrum of Methylammonium Lead Iodide Single-Crystal Perovskites. *Advanced Materials* **28**, 3406-3410 (2016).

77 Chen, Y., Yi, H. T., Wu, X., Haroldson, R., Gartstein, Y. N., Rodionov, Y. I., Tikhonov, K. S., Zakhidov, A., Zhu, X. Y. & Podzorov, V. Extended carrier lifetimes and diffusion in hybrid perovskites revealed by Hall effect and photoconductivity measurements. *Nature Communications* **7**, 12253 (2016).

78 Meggiolaro, D., Motti, S. G., Mosconi, E., Barker, A. J., Ball, J., Andrea Riccardo Perini, C., Deschler, F., Petrozza, A. & De Angelis, F. Iodine chemistry determines the defect tolerance of lead-halide perovskites. *Energy & Environmental Science* **11**, 702-713 (2018).

79 Shi, D., Adinolfi, V., Comin, R., Yuan, M., Alarousu, E., Buin, A., Chen, Y., Hoogland, S., Rothenberger, A., Katsiev, K., Losovyj, Y., Zhang, X., Dowben Peter, A., Mohammed Omar, F., Sargent Edward, H. & Bakr Osman, M. Low trap-state density and long carrier diffusion in organolead trihalide perovskite single crystals. *Science* **347**, 519-522 (2015).

80 Brenner, T. M., Egger, D. A., Kronik, L., Hodes, G. & Cahen, D. Hybrid organic—inorganic perovskites: low-cost semiconductors with intriguing charge-transport properties. *Nature Reviews Materials* **1**, 15007 (2016).

Supplementary Files

This is a list of supplementary files associated with this preprint. Click to download.

- SChenEPCflat1.pdf